Dynamic Wetting for Continuum Hydrodynamics with Multi-Component Lattice Boltzmann Equation Simulation Method.

Timothy J. Spencer[1], A. P. Hollis[1], I. Halliday[1]* and Christopher. M. Care[1].

* Corresponding author: Tel.: ++44 (0)114 2253045; Fax: ++44 (0)114 2253501;
Email: i.halliday@shu.ac.uk
[1]Materials and Engineering Research Institute, Sheffield Hallam University, UK

Abstract We present methodological innovations to the multi-component lattice Boltzmann equation simulation method which allow for the simulation of dynamic contact lines in the continuum approximation. The improvements are set-out and verified by quantitative results. They allow the simulator access to an expanded range of simulation parameters like viscosity, viscosity contrast and interfacial tensions, and to obtain data with low levels of interfacial micro-current activity in the region of the dynamic contact line.

Keywords: Lattice Boltzmann, multi-component flow, wetting.

1 Introduction

The list of areas in which the lattice Boltzmann Equation method (LBM) has widely accepted advantages over traditional methods of CFD is relatively short but geometrically complex flow of multiple, immiscible fluids is close to its top. Such flows are of unquestioned importance in a range of emerging, micro-fluidic technologies, in which wetting plays a crucial role.

This article's main content extends our accurate lattice closure developed over a series of articles [1-3], to the treatment of multiple fluids at a boundary (ie. to a dynamic contact point). We focus here, on quantitative verification of the resulting method but also demonstrate its considerable potential with applications to the viscous mesoscale (the problem of modeling cellular interactions with vessel walls [4]) and, in the inertial regime (the simulation of a novel, micro-fluidic resonator [5]).

The multi-component lattice Boltzmann (MCLB) method considers "diphasic" fluid as a single "background" fluid with a coupled phase field (which varies only near a fluid-fluid interface) in which physical effects of interfacial tension accrue from application of an appropriately designed external force distribution, directed by the state of the phase fields (a process reviewed briefly in section 2). Applications in wetting clearly demand a demonstrably consistent adaptation of this force / coupled phase field methodology in "boundary" simulation lattice sites which are to represent a slipping (section 3) contact line. Section 1 contains a brief discussion of general, background issues and the results of section 4 measure our success.

2 Background

The simulation of complex wetting phenomena is very important in a number of traditional areas of research. Its understanding is complicated by fact that, as a mathematical necessity, there must be tangential fluid slip in the region of a contact between an interface and a boundary.

2.1 Multi-scale modelling In fact, dynamic contact-line (DCL) behaviour may be used to model eg. the effects of the chemical signalling and selectin-mediated pinning, observed in leukocyte attachment to an arterial vessel wall [4], [6]. The inherent complexity of models such as those in references [4] and [6] urges a highly adapted, numerical description and, since signalling effects will be coupled to flow (through diffusion-convection behaviour), it is essential to retain a meso-scale description of the flow. Therefore, we state at the outset that the multi-scale capacity of the model we develop here resides in its ability (i) to interface with the meso-scale (see

section 2.2 below) and (ii) to accommodate suitable, microscopic, models of an effective wetting process. More precisely, in this article, we shall assume that *hydrodynamic assist* of the wetting is negligible, that slip velocity may be described by a slip length model and that the variation of dynamic wetting angle is a known (possibly experimentally determined) function of the local slip velocity, $\theta_W^D = f(v_{slip})$. In the present context, these assumptions are justified on two counts: first, this work concentrates on the development of an underlying multi-scale technique and, second, for the continuum hydrodynamic scales targeted by eg. King et al. [6], absorbed surface layers, typically of a few molecular diameters' thickness, and chemotractant interactions are not explicitly resolved when treating flow.

Notwithstanding our previous remarks, the meso-scale method developed here will couple flexibly to the micro-scale via appropriate models of (i) slip and (ii) dynamic wetting (eg. after King et. al. [6]).

2.2 Meso-scale flow simulation method for externally forced fluid Let us consider the simplest, most popular Lattice Boltzmann Equation (LBE) method, the LBGK variant [7]. Like LBE, LBGK simulation may be considered as a collision and propagation, over a regular lattice with basis vectors (or links) $\underline{c}_i$ and associated weights, t_p, of a single particle distribution function [8]. In the case of multiple, immiscible fluids, considered here a segregation step [9] is added (see section 3).

Pro tem we consider a single fluid. An enhanced LBGK scheme, due to Guo et al. [10], describes bulk fluids *in the presence of a spatially variable external force* as an evolution of a single particle distribution function:

$$f_i^{'} = f_i^{(0)}(\rho,\underline{u}) + \left(1-\frac{\delta_t}{\tau}\right) f_i^{(1)} + \phi_i \qquad (2.2.1)$$

where the "equilibrium "is:

$$f_i^{(0)}(\rho,\underline{u}) \equiv t_p \rho \left(1 + \frac{\underline{u}.\underline{c}_i}{c_s^2} + \frac{\left(c_{i\alpha}c_{i\beta} - c_s^2\delta_{\alpha\beta}\right)u_\alpha u_\beta}{2c_s^2}\right) \qquad (2.2.2)$$

In (2.2.1), a prime denotes a "collided" quantity [8] and the source contribution, ϕ_i is related to the spatially variable external force distribution, $\underline{F}$ [10]:

$$\phi_i = t_p\left(1-\frac{1}{2\tau}\right)\left(\frac{\underline{c}_i - \underline{u}}{c_s^2} + \frac{\underline{c}_i.\underline{u}}{c_s^4}\underline{c}_i\right).\underline{F}. \qquad (2.2.3)$$

In the last equations, all other symbols have their usual meaning. Guo et al. show, by means of a modified Chapman-Enskog (CE) expansion [8] that the macroscopic fluid density and velocity are, respectively, to be obtained from the following moments of the pre-collision particle distribution function with the lattice basis, $\underline{c}_i$:

$$\rho = \sum_i f_i ,$$

$$\rho\underline{u} = \sum_i f_i \underline{c}_i + \frac{\delta_t}{2}\underline{F},. \qquad (2.2.4)$$

and proceed to recover, with modified Chapman-Eskog analysis [8], meso-scale dynamics described by a continuity and Navier-Stokes equation, with external body force, $\underline{F}$ [10].

3 Theoretical Developments

3.1 General Developments We present, in this sub-section, key results which follow directly from the analysis of Guo at al. [10], who assume the usual $\underline{c}_i$ -moments of $f_i^{(0)}(\rho,\underline{u})$ [8,11]. It is implicit, however, that modifications are necessary for moments of $f_i^{(1)} \equiv \left(f_i - f_i^{(0)}(\rho,\underline{u})\right)$. By straightforward, but tedious, algebra it is possible to extract modified relations for $\underline{c}_i$-moments of the pre-collision distribution function $f_i^{(1)}$:

$$\sum_i f_i^{(1)} = 0, \qquad (3.1.1)$$

$$\sum_i f_i^{(1)} c_{i\alpha} = \frac{1}{2}\delta_t F_\alpha, \qquad (3.1.2)$$

$$\sum_i f_i^{(1)} c_{i\alpha} c_{i\beta} = -2\rho c_s^2 \tau S_{\alpha\beta}, \qquad (3.1.3)$$

where, in (3.1.3), we have modified the definition of the fluid strain rate tensor:

$$S_{\alpha\beta} \equiv \frac{1}{2}\left(\partial_\alpha u_\beta + \partial_\beta u_\alpha\right) + \frac{\delta_t}{4\rho c_s^2 \tau}\left(F_\alpha u_\beta + F_\beta u_\alpha\right) \qquad (3.1.4)$$

in which $\underline{u}$ is given by (2.2.4) and $\underline{F}$ is the known external force. Of course, (3.1.1)..(3.1.3) reduce to the usual results [8,11] in the limit $F_\alpha \to 0$. In our target adaptation (the interaction of the interface with a solid boundary), the external force is a sum of two contributions: gravity and an interface force. The latter is used to insert appropriate dynamics (eg. the no-traction condition) and the kinematics (ie. continuity of velocity) appropriate to the continuum interface [9,12]. This, central aspect of the simulation methodology is bound-up with the definition of the fluid component identifying phase field, and so is discussed in the next section.

3.2 Boundary Segregation Scheme In the parent, bulk, MCLB, segregation is designed to be consistent with advection of the component-distinguishing phase field function, optimally to recover continuum regime multi-component hydrodynamics [9,13]: this consistency is strikingly verified by the good agreement achieved recently in a challenging validation against theoretically predicted drop shapes [14]. The interface between a red and blue fluid is identified by constant value contours of phase field function:

$$\rho^N \equiv \left(\frac{R-B}{R+B}\right),$$

in which we define:

$$R \equiv \sum_i R_i, \qquad B \equiv \sum_i B_i, \qquad (3.2.1)$$

where nodal densities, R and B, derive from a "coloured" particle distribution function:

$$f_i = R_i + B_i, \qquad (3.2.2)$$

and, of course, conserve "un-coloured" mass:

$$\rho = R + B. \qquad (3.2.3)$$

When post-collision colour allocation follows d'Ortona et al. [15] and Latva-Koko and Rothman [16]:

$$R_i = \frac{R}{R+B}\left(f_i' + \phi_i\right) - \beta t_p \frac{RB}{R+B}\underline{c}_i.\hat{n},$$
$$\hat{n} \equiv -\frac{\nabla\rho^N}{\left\|\nabla\rho^N\right\|}, \qquad (3.2.4)$$

the dynamics of the phase field [9,13]:

$$\frac{D}{Dt}\rho^N = -\rho\left(\partial_\alpha\partial_\beta u_\beta u_\alpha\right), \qquad (3.2.5)$$

is close to that passive advection required by the kinematic condition of continuum hydrodynamics (since the right hand side of (3.2.5) is small). The surface tension inducing force applied in our LBGK fluid is also determined by ρ^N [12]:

$$F_\alpha = \frac{1}{2}K\sigma\frac{\partial}{\partial x_\alpha}\rho^N, \quad K \equiv \underline{\nabla}.\hat{n} \quad . \qquad (3.2.6)$$

We consider now a set of modifications to this method which facilitate its application to the problem of wetting: that is, we consider the contact region between two immiscible fluids and a solid boundary, depicted in figure 1.

3.2.1 Boundary isotropic derivatives For optimal accuracy and minimum micro-currents [8] it is essential that all derivatives occurring in (3.1.1)..(3.2.3) should be measured using isotropic derivatives [17]. Expressions equivalent to those in ref. [17] (ie. isotropic

and of o(4) accuracy in the lattice basis) may be straightforwardly obtained for positions on the flat boundary of the D2Q9 lattice, depicted in figure 1, simply by constraining expansions in $\underline{c}_i$ to the half-plane which lie in Ω and considering sites further from the boundary [8]:

$$\frac{\partial g}{\partial x_\beta} = \sum_i t_p c_{i\beta}\left(12g(\underline{r}+\underline{c}_i) + 3g(\underline{r}+2\underline{c}_i)\right), \tag{3.2.7}$$

where *g* is some observable parameter and the summation is to be taken over only those "live" link directions which connect to the flow domain, Ω, (see figure 1).

3.2.2 Colour conserving boundary closure
In the situation represented in figure 1, the boundary has a known velocity, $\underline{u}_0$ (which may correspond to slip). We are concerned to populate only live links ($i \neq 1,2,3$) with values of R_i and B_i which are as accurately calculated by the bulk scheme (2.2.1) and conserve, within Ω, masses of both colours.

Importantly, the presence of an external force-inducing, source, term in evolution equation (2.1) disrupts mass conservation on the subset of live links:

$$\Delta M = \sum_{i\neq 5,6,7}\phi_i = \left(1-\frac{1}{2\tau}\right)\underline{F}.\sum_{i\neq 5,6,7} t_p\left(\frac{\underline{c}_i-\underline{u}_0}{c_s^2}+\frac{\underline{c}_i.\underline{u}_0}{c_s^4}\underline{c}_i\right)\neq 0 \tag{3.2.8}$$

Let $R_{in}\left(B_{in}\right)$ denote the total red (blue) mass which propagates onto our boundary node:

$$R_{in} \equiv \sum_{i\neq 1,2,3} R_i\,, \qquad B_{in} \equiv \sum_{i\neq 1,2,3} B_i\,. \tag{3.2.9}$$

Define auxiliary, boundary density, ρ':

$$R_{in} + B_{in} - \Delta M = \sum_{i\neq 1,2,3} f_i^{(0)}\left(\rho', \underline{u}_0\right). \tag{3.2.10}$$

Note, from (3.2.10) and the definition of ΔM:

$$R_{in} + B_{in} = \sum_{i\neq 1,2,3}\left(f_i^{(0)}\left(\rho', \underline{u}_0\right) + \phi_i\right). \tag{3.2.11}$$

Since $f_i^{(0)}\left(\rho', \underline{u}_0\right)$ is always linear in ρ' [8] it is possible to invert (3.2.11), to identify ρ'; for our example of geometry of figure 1:

$$\rho' = \frac{R_{in}+B_{in}}{\sum_{i\neq 1,2,3} f_i^{(0)}\left(1,\underline{u}_0\right)} = \frac{R_{in}+B_{in}}{\left(\frac{10+6u_{0y}-6u_{0y}^2}{12}\right)}\,.$$

Alternative boundary geometries may be similarly treated. For definiteness, suppose that $\underline{u}_0$ has only an *x*-component:

$$\rho' = \frac{6}{5}\left(R_{in}+B_{in}\right). \tag{3.2.12}$$

In fact, equations (3.2.12)..(3.2.13) are sufficient to determine an *o*(1) accurate mass conserving closure for a fluid under external force, from $f_i' \approx f_i^{(0)}\left(\rho', \underline{u}_0\right) + \phi_i$. To obtain the desired *o*(2) accurate closure, however, it is necessary to determine appropriate $f_i^{(1)}$s for live links. This is made possible by the system of $(D+1)(D+2)/2$ (where *D* denotes dimensionality) simultaneous equations *after* (3.1.1)..(3.1.3) of section (3.1), in which the first equation (only) has been adjusted to underwrite mass conservation:

$$\begin{aligned}
&\sum_{i\neq 5,6,7} f_i^{(1)} = 0\,,\\
&\sum_i f_i^{(1)} c_{i\alpha} = \frac{1}{2}\delta_t F_\alpha\,,\\
&\sum_i f_i^{(1)} c_{i\alpha} c_{i\beta} = -2\rho' c_s^2 \tau\, S_{\alpha\beta}\,.
\end{aligned} \tag{3.2.13}$$

(Restricting the summation in zeroth moment in the first equation (3.2.13) above conserves mass on live links of the geometry in figure 1.) Previously, we have solved this under-specified system of 6 simultaneous equations in unknown $f_i^{(1)}$s by recourse to a choice of "free variables", a process complicated by

several considerations [1-3].
A considerable improvement in stability and simplicity may be achieved, and the need arbitrarily to select free variables removed, by solving the under-specified system of equations (3.2.13) by the method of singular value decomposition (SVD) [18]. System (3.2.13) may be written in non-square matrix form:

$$\underline{\underline{M}}\ \underline{f^{(1)}} = \underline{b},$$
$$\underline{f^{(1)}} \equiv \left(f_0^{(1)} \quad f_1^{(1)} \quad \ldots \quad f_8^{(1)}\right)^T,$$
$$\underline{b} \equiv \frac{\delta_t}{2}\left(0 \quad F_x \quad F_y \quad -kS_{xx} \quad -kS_{yy} \quad -kS_{xy}\right)^T$$

in which system we have defined:

$$k \equiv \frac{4\rho' c_s^2 \tau}{\delta_t} S_{\alpha\beta}.$$

SVD allows one to establish a pseudo-inverse matrix $\underline{\underline{M}}^{-1}$. SVD is a standard method for decomposing non-square matrices, which may be regarded as a generalization of the eigenvector decomposition commonly used on square matrices. Our solution for $\underline{f^{(1)}}$ obtained in this way is described in a basis comprised of the right singular vectors associated with $\underline{\underline{M}}$ and contains no contribution from the other three, which form the null-space of $\underline{\underline{M}}$. It is the latter choice which essentially provides the remaining three conditions needed to close the incomplete description furnished by equations (3.2.13). The solution for the live links of figure 1 is:

$$\begin{pmatrix} f_0^{(1)} \\ f_1^{(1)} \\ f_2^{(1)} \\ f_3^{(1)} \\ f_4^{(1)} \\ f_8^{(1)} \end{pmatrix} = \frac{1}{36}\begin{pmatrix} 0 & -5 & -12 & -2 & 0 \\ -3 & 4 & 6 & 4 & -3 \\ 0 & 1 & -4 & 10 & 0 \\ 3 & 4 & 6 & 4 & 9 \\ 3 & -2 & 6 & -8 & 0 \\ -3 & -2 & 6 & -8 & 0 \end{pmatrix}\begin{pmatrix} \delta_t F_x \\ \delta_t F_y \\ \rho' c_s^2 \varpi S_{xx} \\ \rho' c_s^2 \varpi S_{yy} \\ \rho' c_s^2 \varpi S_{xy} \end{pmatrix} \qquad (3.2.14)$$

The strains in the above system were evaluated by fourth-order accurate isotropic finite differences.
With the means of calculating boundary densities determined, we turn now to the problem of allocating colour mass at a boundary interfacial site, in such a way as to maintain consistency with the core scheme and to conserve colour in the flow domain. Stated relative to our chosen geometry, colour conservation requires that the post collision, post segregation red and blue densities assigned to live links should give:

$$\sum_{i\neq 5,6,7} R_i' = R_{in}, \quad \sum_{i\neq 5,6,7} B_i' = B_{in},$$
$$\sum_{i\neq 5,6,7}\left(f_i' + \phi_i\right) = R_{in} + B_{in}. \qquad (3.2.15)$$

Let R' and B' be fictitious boundary node red and blue densities which will satisfy mass conservation. We wish to segregate the boundary node in a manner which is consistent with the bulk node. We obtain an equation in R' and B' by substituting, into the first equation (3.2.15) using bulk segregation formula (3.2.4); straightforwardly we obtain:

$$\frac{R'}{R'+B'}\left(R_{in}+B_{in}\right) + \frac{R'B'}{R'+B'}\beta\,\hat{n}.\left(\sum_{i\neq 5,6,7}\left(t_p\,\underline{c}_i\right)\right) = R_{in} \qquad (3.2.16)$$

The summation in the second term of the left hand side of (3.2.16) may be evaluated for any boundary node geometry. For the case of figure 1:

$$\underline{n}.\left(\sum_{i\neq 5,6,7}\left(t_p\,\underline{c}_i\right)\right) = \frac{1}{6}n_y, \qquad (3.2.17)$$

where, n_y is the y-component of the interfacial colour field. Since $\rho' = R' + B'$, we obtain, using (3.2.12) (still for our example geometry of Figure 1, note) an expression for ρ' which may be evaluated readily:

$$\rho' = R' + B' = \frac{6}{5}\left(R_{in} + B_{in}\right). \qquad (3.2.18)$$

With the above simple result and equations (3.2.17) and (3.2.16), we obtain, by straightforward algebra:

$$(\beta n_y)R'^2 - \rho'(5+\beta n_y)R' - 6\rho' R_{in} = 0\,, \qquad (3.2.19)$$

solution of which quadratic yields a value of R'. With B' determined directly, using (3.2.18), the segregation formula (3.2.4) may be applied on the boundary as:

$$R_i(\underline{r},t) = \frac{R'}{R'+B'}\left(f_i' + \phi_i\right) + \beta t_p \frac{R'B'}{R'+B'}_i\, \hat{n}.\underline{c}_i$$

4 Results

In the simulation results reported, the model outlined in section 3 was used. Where a simple model of DCL slip was necessary, a slip-length, *b*, was employed to obtain a tangential boundary slip velocity, the normal component following from kinematical considerations:

$$u_{0y} = u_{y\ wall} = 0 \quad , \quad u_{0x} = b\left[\frac{\partial u_x}{\partial y}\right]_{y=0} .$$

Figures 2 and 3 relate to a semi-infinite meniscus, parameterized for the air-water interface under gravity. We have reported elsewhere the method of MCLB surface tension parameterization [19] used to obtain the data of Figure 2, which shows the micro-current generated by the method. It is important to note that the intensity of this spurious flow, where the interface approaches the boundary, is comparable to its value close to the bulk interface (which is indicated by the solid line). Since the bulk algorithm has a very low interfacial micro-current and an ability to reach large interfacial tensions, this result underlines the utility of the method.

Figure 3 shows the excellent agreement achieved between our method and the predicted meniscus shape [20] of the air water interface and contact angle. Importantly, the result for figure 3 is insensitive to the value of the interface thickness parameter, β. Figure 4 shows a potential application of our method, in the area of biological micro-fluidics, where the motion of a leukocyte, rolling on a vessel wall is, for purposes of modelling, widely represented as that of an immiscible drop of one fluid, suspended in a second fluid (the point of attachment is then represented as a DCL). The contours in figure 4 represent contours of constant instantaneous value of the rectangular stream function. The drop, with viscosity contrast 7, is "rolling" on the boundary at small Reynolds number-generally a challenging and important regime for our method to access, as small interfacial micro-current flow will not obscure the velocities. The quality of these data and, in particular, the resolution of the stream function in the contact underscore the potential utility of the method. Figure 5 is a application of the method to the inertial regime of flow, and depicts the flow field, phase field and rectangular stream function in the cavity of a novel micro-fluidic device [4].

The use of SVD to close the description (see section 3 and equation (3.2.14)) considerably enhances the stability of the resulting method and increases the range of collision parameter, τ, (and hence Reynolds and Capillary number) accessible. This outcome will be reported in more detail elsewhere.

5 Conclusion

We have presented methodological innovations to the multi-component lattice Boltzmann equation simulation method which allow for the multi-scale simulation of dynamic contact lines in the continuum approximation. The improvements are set-out and are supported by the results. They allow the simulator access to an expanded range of simulation parameters like viscosity, viscosity contrast, interfacial tension and characteristic velocity. Simulation at low values of characteristic velocity is made possible by the low levels of interfacial micro-current activity in the region of the dynamic contact line produced by our method.

6 References

[1] I. Halliday, C. M. Care, L. A. Hammond, A. Stevens. J Phys A: Math. Gen 35 (2002) pp157.
[2] A. P. Hollis, I. Halliday and C. M. Care, J. Phys. A: Math. Gen. **39** (2006) pp10589.
[3] A. P. Hollis, I. Halliday and C. M. Care**,** J. Comp. Phys**.** 227 (17) (2008) pp8065.
[4] S. V. Lishchuk, I. Halliday, M. Atherton, C. M. Care, M. W. Collins, D. Evans , P. C. Evans, D. R. Hose, A. W. Khir, R. Krams, P. V. Lawford, V. Ridger, Y. Ventikos, D. C. Walker , P. N. Watton. "Multi-scale Interaction of Flow and the Artery Wall." In 2nd Micro and Nano Flows Conference Proceedings.
[5] A. Clarke, N. Dartnell, T. J. Spencer, C. M. Care and I. Halliday, Submitted PRE (2009).
[6] J. R. King and J. M. Oliver *Euro J Appl Maths* **16,** (2005) pp519
[7] Y. H. Qian, D. D'Humieres and P. Lallemand, Europhys. Lett. 17 (1992) pp479.
[8] S. Succi, *The Lattice Boltzmann Equation for Fluid Dynamics and Beyond* (Oxford University Press, ISBN: 978-0-19-850398-9).
[9] I. Halliday, C. M. Care and A. P. Hollis Phys. Rev. E. 76, 026708 (2007).
[10] Z. Guo, C. Zheng and B. Shi, Phys. Rev. E. 65, 046308 (2002).
[11] S. Hou, Q. Zou, S. Chen, G. Doolen and A. C. Cogley. J. Comp. Phys. 118 (1995) pp329.
[12] S. V. Lishchuk, C. M. Care and I. Halliday, Phys. Rev. E, 67, 036701 (2003).
[13] A. P. Hollis, I. Halliday and R. Law, Phys. Rev. E 76, 026709 (2007).
[14] I. Halliday, C. M. Care I. Halliday, T. J. Spencer, and C. M. Care, Phys. Rev. E, 79, 016706 (2009)
[15] U. d'Ortona, D. Salin, M. Cieplak, P. B. Rybka and J. R. Banavar, Phys. Rev. E, 51 pp3718 (1995)
[16] M. Latva-Kokko and D. H. Rothman, Phys. Rev. E, 71 056702 (2005)
[17] I. Halliday, C. M. Care, R. Law and A. P. Hollis, Phys. Rev. E, 73 (1), 056708 (2006)
[18] C. D. Cantrell, *Modern Mathematical Methods for Physicists and Engineers* Cambridge University Press (2000)
[19] S. V. Lishchuk, I Halliday and C M Care Phys Rev E 77 (3) (E036702) (2008)
[20] G. K. Batchelor, *Introduction to Fluid Mechanics* Cambridge

7 Figures

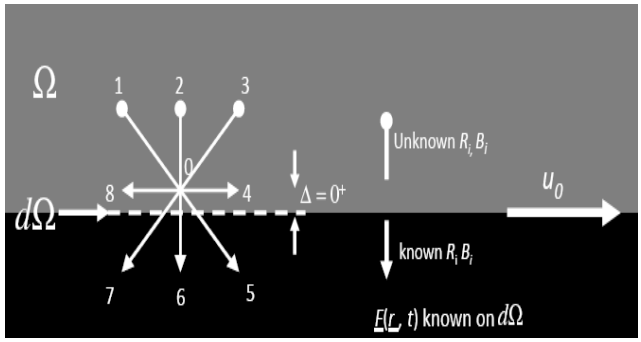

Figure 1 A D2Q9 lattice node located in a boundary. The link indexing it that referred to in the text. Horizontal links 0, 4 and 8 are located in the fluid. Links 5, 6 and 7 are cut by the boundary, which is supposed to move with velocity $\underline{u_0}$. Fluid (solid) is the grey (black) region.

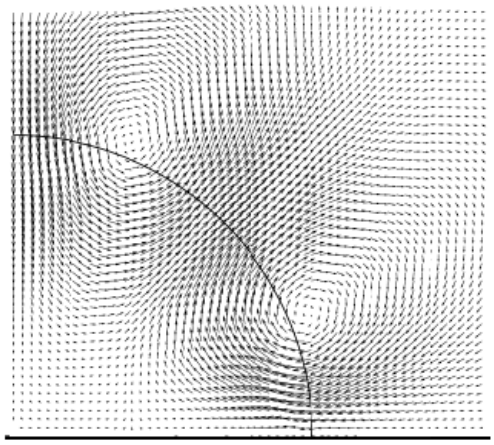

Figure 2 Velocity field vectors for the spurious interfacial flow or "micro-current" at steady state. The heavy solid line indicates the flat boundary, the light solid line is the location of the curved interface of a drop, defined by the (sub-lattice) $\rho^N = 0$ contour, plotted, always defines the centre of the interface. Notably, the spurious interfacial micro-current circulations, always present at the interface, is seen to be slightly smaller in intensity close to the boundary.

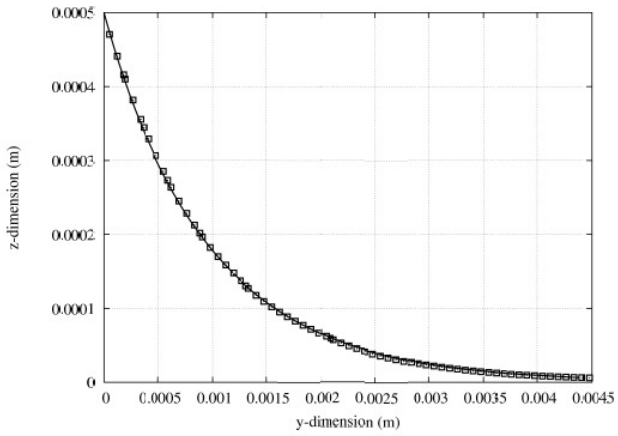

Figure 3 Computed (points) and predicted (continuous line) position of a semi-infinite air-water meniscus. Simulation data is clearly in excellent agreement with theory. As in figure 2, the (sub-lattice) $\rho^N = 0$ contour, plotted, always defines the centre of the interface.

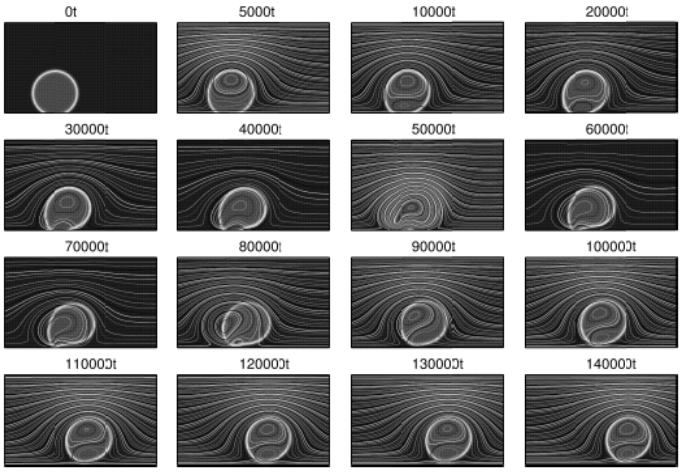

Figure 4 A liquid drop model of leukocyte detachment (reverse of attachment). The flow is viscous-dominated. Light-shaded (leukocyte) or light (plasma) phases are overlaid by contours of constant value in the rectangular stream function [20] Images are labelled by time measured in lattice units.

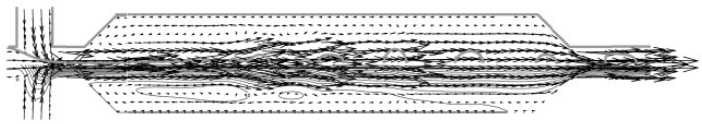

Figure 5 Inertial flow (Re = o(10^2)) within the chamber of a novel "micro-fluidic resonator". The velocity field, phase field and rectangular stream function are all represented in this figure. Three streams of two immiscible fluids enter the chamber on the left: this "inlet geometry" is similar to other flow-focusing devices. Simulations confirm experimental observation of both dripping and jetting modes within the device chamber, with the transition between these two regimes being controlled by flow rates and Re. Crucially, in the jetting mode, the jet is observed to break-up into very regular drops, within the cavity. Simulations and experiments conducted in similar inlet geometry but without the channel constriction on the right (ie. with the stabilizing influence of the cavity removed) exhibit a loss of this resonance [5].